THE JOURNAL OF PHYSICAL CHEMISTRY B

Article

Cite This: J. Phys. Chem. B 2018, 122, 1261−1267

pubs.acs.org/JPCB

Glycerol Hydrogen-Bonding Network Dominates Structure and Collective Dynamics in a Deep Eutectic Solvent

A. Faraone,*[,†] D. V. Wagle,[‡] G. A. Baker,*[,‡] E. C. Novak,[§] M. Ohl,[⊥] D. Reuter,[#] P. Lunkenheimer,[#] A. Loidl,[#] and E. Mamontov*[,∥]

[†]NIST Center for Neutron Research, National Institute of Standards and Technology Gaithersburg, Gaithersburg, Maryland 20899, United States

[‡]Department of Chemistry, University of Missouri-Columbia, Columbia, Missouri 65211, United States

[§]Department of Materials Science and Engineering, University of Tennessee, Knoxville, Tennessee 37996, United States

[∥]Neutron Scattering Division, Neutron Sciences Directorate, Oak Ridge National Laboratory, Oak Ridge, Tennessee 37831, United States

[⊥]Jülich Center for Neutron Science, Forschungszentrum Jülich GmbH, Jülich 52425, Germany

[#]Experimental Physics V, Center for Electronic Correlations and Magnetism, University of Augsburg, Augsburg 86159, Germany

Supporting Information

ABSTRACT: The deep eutectic solvent glyceline formed by choline chloride and glycerol in 1:2 molar ratio is much less viscous compared to glycerol, which facilitates its use in many applications where high viscosity is undesirable. Despite the large difference in viscosity, we have found that the structural network of glyceline is completely defined by its glycerol constituent, which exhibits complex microscopic dynamic behavior, as expected from a highly correlated hydrogen-bonding network. Choline ions occupy interstitial voids in the glycerol network and show little structural or dynamic correlations with glycerol molecules. Despite the known higher long-range diffusivity of the smaller glycerol species in glyceline, in applications where localized dynamics is essential (e.g., in microporous media), the local transport and dynamic properties must be dominated by the relatively loosely bound choline ions.

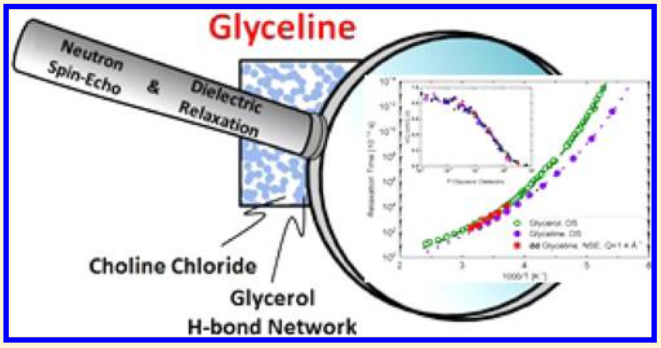

INTRODUCTION

Unlike traditional room-temperature ionic liquids, their recently discovered low-cost, biodegradable, nontoxic counterparts, referred to as deep eutectic solvents (DES's), are composed of both ionic and molecular (neutral) constituents.[1−3] In 2003, Abbott and co-workers were the first to report on contemporary DES's prepared by mixing, in appropriate stoichiometry, a hydrogen bond acceptor (HBA) such as the high-melting organic salt choline chloride (melting point, mp: 302 °C) with a suitable hydrogen bond donor (HBD) species like urea (mp: 133 °C).[1] Several formulations for DES's involving diverse HBD/HBA combinations have since emerged, with choline chloride featuring prominently as the quaternary ammonium salt of choice, coupled with a variety of HBDs, including assorted carboxylic acids, amides, phenols, and glycols. As emerging sustainable media, DES's are already finding applications in a multitude of areas, including morphologically controlled nanoparticle synthesis,[3−7] metal−organic frameworks,[8−10] thin-film electrodeposition,[11−13] gas capture,[14−20] fossil fuel desulfurization,[21−23] micellar chemistry,[24−27] porous carbons,[28,29] organic synthesis,[30] liquid extraction,[22,31] biodiesel production,[32] biomass treatment,[33−35] and DNA/RNA chemistry.[36,37]

Recently, there has been a significant push to gain deeper insight into the structure, dynamics, and molecular interactions present within DES's using a wealth of computational methods.[38−40] Computational efforts have revealed that the addition of HBDs results in significant moderation of the cation−anion interaction in a complex manner within the DES.[41] These studies paint a picture of DES formation being accompanied by hydrogen-bond-directed charge transfer processes to yield transient cage-like formation and nanoscale ordering entailing segregation of the ionic and molecular domains.[38,42] The hydrogen-bonding network is essential for eutectic formation and strongly influences the local structure and dynamics within DES's. Thus, a rigorous understanding of the complexities of the hydrogen-bonding network is paramount to the rational future design of tailored and chemically diverse DES's. Recently, neutron scattering (e.g., small-angle,

Received: November 13, 2017
Revised: January 2, 2018
Published: January 16, 2018

DOI: 10.1021/acs.jpcb.7b11224
J. Phys. Chem. B 2018, 122, 1261−1267

total, and quasi-elastic neutron scattering (QENS)) techniques have been leveraged to probe the microscopic details of liquid structure and dynamics within DES's and their binary mixtures with water, offering valuable insight into the underlying nanostructure, disorder, clustering (i.e., domain and transient cage formation), charge transfer, and phase behavior.[43−48] Key information regarding the behavior and self-assembly of polymers, proteins, and micelles in DES's is also accessible from neutron scattering studies.[27,49−52] A recent QENS study on the microscopic dynamics within the DES glyceline (1:2 choline chloride/glycerol) revealed that choline experiences a spacious local environment and exhibits less spatially constrained short-range diffusion dynamics,[48] despite its smaller long-range translational diffusivity compared to the slightly smaller molecular component, glycerol.[53−55] The collective microscopic dynamics within DES's, which are most directly linked to the properties associated with the hydrogen-bonding network between the DES components, have remained unexplored as pulsed-field gradient NMR spectroscopy and QENS experiments probe the single-particle diffusion dynamics.[48,53−55] In response to this drawback, we report on a neutron spin-echo (NSE) study paired with dielectric spectroscopy measurements that help elucidate the collective microscopic dynamics within the DES glyceline. A detailed understanding of the glyceline collective dynamics is made possible by the application of NSE that mostly probes the coherent neutron scattering signal of glyceline samples synthesized with different hydrogen−deuterium compositions. The four samples used in this study are denoted hh (hydrogenated choline chloride/hydrogenated glycerol), hd (hydrogenated choline chloride/deuterated glycerol), dh (deuterated choline chloride/hydrogenated glycerol), and dd (deuterated choline chloride/deuterated glycerol).

METHODS

Broadband Dielectric Spectroscopy. For the dielectric measurements, we combined two experimental techniques to determine the complex dielectric permittivity and conductivity in the frequency range $10^0 \leq \nu \leq 2.5 \times 10^9$ Hz. In both cases, parallel-plate capacitors (diameter 2 or 19 mm, plate distance ≤ 100 μm) were filled with the liquid sample material. The low-frequency measurements at $10^0 \leq \nu \leq 10^6$ Hz were performed using a frequency-response analyzer (Novocontrol Alpha-A analyzer). At higher frequencies, $10^6 \leq \nu \leq 2.5 \times 10^9$ Hz, a coaxial reflectometric technique was used employing an impedance analyzer (Agilent E4991A). Cooling and heating were achieved by a N_2 gas heating system (Novocontrol Quatro). Further details of this can be found in previously reported works.[56,57]

Chemicals. Trimethyl-d_9-amine, ethylene-d_4 oxide, hydrochloric acid, and choline chloride were purchased from Sigma-Aldrich (St. Louis, MO). Glycerol-d_8 was acquired from C/D/N Isotopes Inc. (Quebec, Canada).

Preparation of Four Glyceline Samples of Variable Deuteration States. *Synthesis of Choline-d_{14} Chloride.* The reaction and reaction setup for choline-d_{14} chloride have been described in the Supporting Information (SI).

Step 1: Preparation of Trimethyl-d_9-ammonium Chloride. First, 4.336 g of a 37% mass fraction aqueous solution of HCl was added to a cylindrical flask equipped with a valve side arm and which already contained a poly(tetrafluoroethylene)-coated stir bar and 5 g of distilled water. The flask was tightly sealed with a rubber septum and chilled in an ice bath. Trimethyl-d_9-amine gas (3.04 g, 1.02 equiv) was transferred from a pressurized cylinder to the reaction mixture via a Tygon tube (R-3603) connected to a 1 mL syringe (Sigma-Aldrich, Z-683531) terminated with a stainless steel needle (Sigma-Aldrich, Z-116149). The reaction mixture was stirred for 2 h.

Step 2: Preparation of Choline-d_{13} Chloride. The side arm of the reaction flask was then connected to an ethylene-d_4 oxide (EO-d_4) cylinder via Tygon tubing. The reaction flask was chilled to −80 °C, and the valves of the reaction flask and the ethylene-d_4 oxide cylinder were gradually opened to allow for EO-d_4 transfer and condensation. The valves were then closed, and the reaction flask was allowed to naturally warm to room temperature, followed by heating to 75 °C for 1 h. The flask was cooled to room temperature, and the EO-d_4 transfer was repeated several times until the EO-d_4 cylinder had lost a total of 1.68 g of mass. Following reaction, water was removed from the reaction mixture by rotary evaporation (4.67 Hz, 8 mbar, 78 °C) to yield crude choline-d_{13} chloride. The choline-d_{13} chloride was purified by recrystallization using ethanol before proceeding.

Step 3: Preparation of Choline-d_{14} Chloride. The recrystallized choline-d_{13} chloride was further deuterated to choline-d_{14} chloride via three H−D exchange cycles performed by dissolving choline-d_{13} chloride in D_2O, followed by rotary evaporation. The exchange was initially carried out by dissolving 4.2 g of choline-d_{13} chloride in 10 mL of D_2O (99.9 atom % D, Aldrich), followed by rotary evaporation. This was repeated twice to yield 4.2 g of choline-d_{14} chloride. The overall yield of choline-d_{14} chloride with respect to the amount of EO-d_4 was 79%.

^{13}C NMR (125 MHz, D_2O): δ 54.79 (m, CD_2), 52.85 (m, CD_2), 43.70 (m, CD_3).

Glyceline mixtures with varying degrees of deuteration were synthesized according to previously reported procedures.[48]

Neutron Scattering Experiments. Neutron scattering signal can be divided into a coherent and an incoherent component. The coherent component contains information of the relative position and motions of the nuclei in the sample, whereas the incoherent part, which does not contain any structural information, can be used to measure the single-particle dynamics of the scattering entities, hydrogen atoms in particular. Coherent scattering does not change the spin of the incoming neutron, whereas incoherent scattering has a 2/3 probability of flipping the neutron spin and 1/3 probability of not altering it. Thus, keeping in mind that the neutron spin only has two possible states, namely, + and −, using a polarized neutron beam and an instrument equipped with a spin analyzer device, it is possible to experimentally separate the coherent and incoherent components of the scattering signal. This is achieved by performing measurements of the scattering signal after the analyzer, with opposite polarizations of the incoming neutron beam, which can be obtained with the use of an opportune neutron spin π flipper (see SI for further information).

NSE spectrometers utilize the neutron spins as an internal clock to perform very precise measurement of the distribution of velocity changes experienced by the neutrons after the scattering event. It directly provides the normalized intermediate scattering function (ISF), $I(Q, t)/I(Q, 0)$. Although NSE spectrometers employ a polarized incoming neutron beam because the signal is encoded in the neutron spin itself, they are not able to separate the coherent and incoherent components

DOI: 10.1021/acs.jpcb.7b11224
J. Phys. Chem. B 2018, 122, 1261−1267

to the scattering; instead, the signal measured by spin-echo is a combination of the coherent and incoherent ISFs

$$\frac{I(Q,t)}{I(Q,0)} = \frac{I^{\mathrm{coh}}(Q,t) - \frac{1}{3}I^{\mathrm{incoh}}(Q,t)}{I^{\mathrm{coh}}(Q,0) - \frac{1}{3}I^{\mathrm{incoh}}(Q,0)}$$

"Combination" Scattering. Because of the length scale and time scale of relevance, there is no neutron scattering instrument currently capable of measuring the quasi-elastic coherent signal in the hd or dh samples without significant contamination from the incoherent scattering. It would be possible to perform an analysis of the data considering the presence of both the coherent and incoherent contributions; however, such an approach would rely on complex analysis methods and on a number of assumptions and approximations, even with the support of the measurements on samples with different isotopic compositions. However, within the approximation that the incoherent scattering arises solely from the hydrogen atoms in the sample, it is possible to opportunely combine the scattering from the four samples investigated here to obtain a scattering signal almost entirely coherent in character[58,59]

$$S^{\mathrm{CG}}(Q) = \frac{14}{13}S^{\mathrm{hd}}(Q) + \frac{16}{10}S^{\mathrm{dh}}(Q) - \frac{109}{65}S^{\mathrm{dd}}(Q) - S^{\mathrm{hh}}(Q) \approx S^{\mathrm{CG}}_{\mathrm{coh}}(Q) \quad (1)$$

Here, the prefactors are chosen in such a way as to cancel out the incoherent contributions from the hydrogens as well as those arising from the C, O, N, and Cl atoms. Assuming that the hydrogen atoms of the same molecules are indistinguishable from each other (an approximation supported by the fact that at the Q values analyzed here, the relevant length scales are larger than the intermolecular distance), $S^{\mathrm{CG}}_{\mathrm{coh}}$ is the weighted sum of the structure factors for the correlation between the hydrogen atoms in the choline molecules with respect to each other, $S^{\mathrm{CHCH}}_{\mathrm{coh}}$, in the choline molecules with respect to the ones in the glycerol molecules, $S^{\mathrm{CHGH}}_{\mathrm{coh}}$, and in the glycerol molecules with respect to each other, $S^{\mathrm{GHGH}}_{\mathrm{coh}}$

$$S^{\mathrm{CG}}_{\mathrm{coh}}(Q) = [(13b^{\mathrm{D}}_{\mathrm{coh}} - b^{\mathrm{H}}_{\mathrm{coh}})(-b^{\mathrm{D}}_{\mathrm{coh}} + b^{\mathrm{H}}_{\mathrm{coh}})]S^{\mathrm{CHCH}}_{\mathrm{coh}}(Q) + [224b^{\mathrm{D}}_{\mathrm{coh}}(-b^{\mathrm{D}}_{\mathrm{coh}} + b^{\mathrm{H}}_{\mathrm{coh}})]S^{\mathrm{CHGH}}_{\mathrm{coh}}(Q) + [(60b^{\mathrm{D}}_{\mathrm{coh}} - 36b^{\mathrm{H}}_{\mathrm{coh}})(-b^{\mathrm{D}}_{\mathrm{coh}} + b^{\mathrm{H}}_{\mathrm{coh}})]S^{\mathrm{GHGH}}_{\mathrm{coh}}(Q)$$

It is expected that the three dynamic structure factors, $S^{\mathrm{CHCH}}_{\mathrm{coh}}$, $S^{\mathrm{CHGH}}_{\mathrm{coh}}$, and $S^{\mathrm{GHGH}}_{\mathrm{coh}}$, are determined by the relative positions of the center of mass of the glycerol and choline molecules, although orientational contributions might also play a minor role.

Equation 1 can be extended to the time domain

$$I^{\mathrm{CG}}(Q,t) = \frac{14}{13}I^{\mathrm{hd}}(Q,t) + \frac{16}{10}I^{\mathrm{dh}}(Q,t) - \frac{109}{65}I^{\mathrm{dd}}(Q,t) - I^{\mathrm{hh}}(Q,t) \approx I^{\mathrm{CG}}_{\mathrm{coh}}(Q,t)$$

Thus, the normalized ISF, $I^{\mathrm{CG}}_{\mathrm{coh}}(Q,t)/I^{\mathrm{CG}}_{\mathrm{coh}}(Q,0)$, can be measured using NSE combining the data from the measurements of the four glyceline samples investigated, as detailed in the SI.

RESULTS AND DISCUSSION

Figure 1 shows the temperature dependence of the microscopic relaxation times of glyceline. The α-relaxation times from

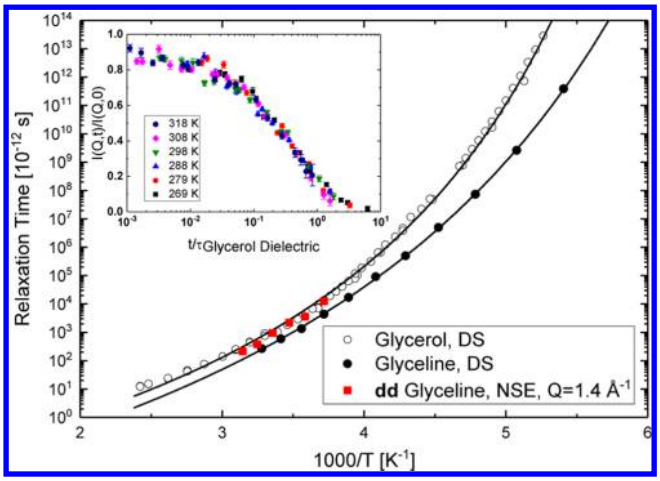

Figure 1. Open circles: glycerol relaxation times measured by dielectric spectroscopy and the corresponding VFT fit (solid line, ref 60). Filled circles: glyceline relaxation times measured by dielectric spectroscopy and the corresponding VFT fit (solid line). Red symbols: glyceline average relaxation times, $\langle\tau\rangle$, obtained from the NSE data. Inset: glyceline NSE $I(Q,t)$ data measured at various temperatures and plotted as a function of Fourier time scaled by the dielectric relaxation times of glycerol.

broadband dielectric spectroscopy measurements on hydrogenated glyceline (black closed circles, see SI) are compared to those of hydrogenated glycerol (open circles).[60] A Vogel–Fulcher–Tammann (VFT) fit of the dielectric relaxation data, $\tau = \tau_0 \exp(DT_0/(T - T_0))$, gives $\tau_0 = 4 \times 10^{-15} \pm 2 \times 10^{-15}$ s, $D = 16 \pm 1$, and $T_0 = 132 \pm 3$ K for glycerol and $\tau_0 = 8 \times 10^{-16} \pm 6 \times 10^{-16}$ s, $D = 21 \pm 3$, and $T_0 = 113 \pm 4$ K for glyceline, which correspond to glass transition temperatures (T_g) of about 185 and 175 K, respectively.[60] The VFT equation is customarily applied to the so-called "fragile" glass formers with strongly non-Arrhenius temperature dependence of the relaxation characteristics.[61]

Glyceline is known to be less viscous than glycerol, which makes its use advantageous in applications where the viscosity of pure glycerol would be prohibitively high, hampering chemical transport. The viscosity of glyceline is 281 cP at 298 K, whereas the viscosity of glycerol is around 1200 cP at room temperature.[62] Moreover, for various compositions of a choline chloride mixture with glycerol (i.e., 0.05, 0.10, 0.15, 0.20, 0.25, 0.30, and 0.33 mol fraction of choline chloride), the lowest viscosity was observed for 0.33 mol fraction of choline chloride (i.e., 1:2 choline chloride/glycerol, in other words, glyceline).[53] Indeed, the dielectric data indicate that the α-relaxation dynamics of glyceline is faster than that of glycerol. Around room temperature, the ratio between the dielectric relaxation times for glyceline and glycerol matches the ratio of the viscosities of the two liquids. At the same time, the long-range single-particle translational diffusivities, as measured by NMR, of the choline ion and glycerol molecule in glyceline have the same temperature dependence[1] from 298 to 328 K and do not significantly differ from the diffusivity of pure glycerol.[63] These experimental findings suggest the crucial role played by the collective dynamics and hydrogen bonding in determining the transport properties of the system.

DOI: 10.1021/acs.jpcb.7b11224
J. Phys. Chem. B 2018, 122, 1261−1267

To probe such collective dynamics, NSE measurements were performed on the dd glyceline sample at the position of the first structural maximum, $Q = 1.4$ Å^{-1} (symbols in Figure 2), where

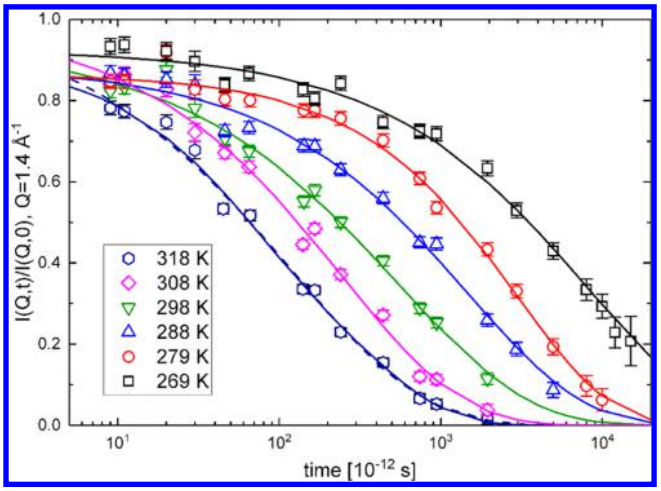

Figure 2. Glyceline relaxation behavior measured by NSE for the dd sample at $Q = 1.4$ Å^{-1} (symbols) and their Kohlrausch–Williams–Watts fits (solid lines). For 318 K, an alternative fit with a two-component model is also shown (dashed line).

$Q = \frac{4\pi}{\lambda}\sin(\theta/2)$ is the exchanged wavevector, λ is the incoming neutron wavelength, and θ is the scattering angle. The data were fitted by the Kohlrausch–Williams–Watts, or stretched-exponential, function, $I(Q, t)/I(Q, 0) = A\exp[-(t/\tau)^{\beta}]$, assuming that the scattering signal is completely dominated by the structural relaxation (solid lines). The deduced average relaxation times, $\langle\tau\rangle = [\tau\Gamma(1/\beta)]/\beta$, are shown as red closed squares in Figure 1. They are about a factor of 3 faster than the NSE results obtained in the past for pure glycerol, with a similar temperature dependence in the investigated range.[64] In this respect, the effect of the addition of choline chloride is essentially to plasticize the glycerol hydrogen-bonded network. However, the NSE relaxation times for glyceline nearly coincide with the pure glycerol, not glyceline, dielectric relaxation time curve, as can be seen in Figure 1. At the highest temperatures, some minor deviations of the two data sets are observed. For 318 K, we demonstrate that that this discrepancy vanishes, when assuming a two-component model, $I(Q, t)/I(Q, 0) = A(p\exp[-(t/\tau_1)^{\beta}] + (1 - p)\exp[-(t/\tau_2)^{\beta}])$, to fit the experimental data (dashed line in Figure 2).[65] The second relaxation with a spectral weight of $(1 - p)$ could be an indication of the fast dynamics known to be present in all glass formers.[66] The α relaxation time resulting from this fit would fully agree with the dielectric relaxation time of glycerol at this temperature. However, as the experimental data do not reveal clear evidence for two-step decay, the significance of such an analysis is limited and no meaningful values for τ_2 can be deduced. The inset of Figure 1 shows the superimposed dd glyceline NSE data measured at various temperatures (see below) and rescaled to the main dielectric relaxation time of glycerol at a given temperature. The data collapse onto a universal curve independent of measurement temperature, again demonstrating that the NSE glyceline data are governed by the same dynamics as the dielectric results on glycerol.

To obtain insights into the structural and dynamic properties of the ionic and molecular nanodomains in glyceline, polarized diffraction data (spin-flip vs no spin-flip) were collected at the NSE spectrometer for all four samples of variable deuteration states, allowing the separation of coherent and incoherent scattering, as presented in Figure 3.

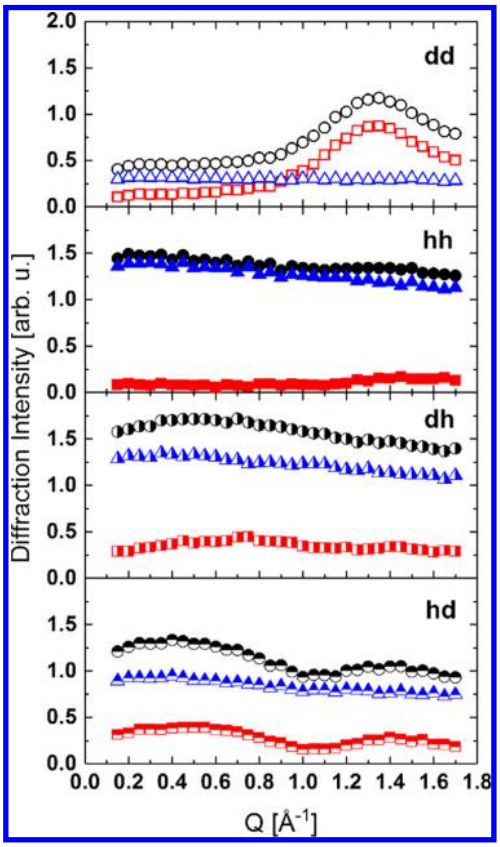

Figure 3. Coherent (red squares), incoherent (blue triangles), and total (black circles) scattering signals obtained from polarized diffraction data (spin-flip vs no spin-flip) for glyceline samples of variable deuteration states. The error bars are within the symbols.

In addition to the predominantly coherently scattering dd sample and predominantly incoherently scattering hh sample, the first structural maximum at ≈1.4 Å^{-1} in the coherent (and thus also total) diffraction spectra is readily seen for the hd sample, but not for the dh sample. Therefore, it is predominantly the glycerol species that form a structural network in glyceline, which gives rise to the coherent diffraction pattern. Because diffraction data correspond to $I(Q, t = 0)$, our conclusion extends to the dynamic NSE data; it is the glycerol component of glyceline that gives rise to the coherent relaxation dynamics measured by NSE. The choline component does not contribute significantly to the coherent microscopic dynamics of glyceline. Moreover, the hd and dh samples show a coherent signal feature centered at $Q^{CG} \approx 0.5$ Å^{-1}, which clearly indicates nanoscopic structuring between glycerol and choline over a length scale on the order of $l^{CG} \approx 2\pi/Q^{CG} = 12.6$ Å. This value is larger than the choline ion size but comparable to the size of the entity, as identified by molecular dynamics simulations,[48] formed by two glycerol molecules and one choline cation hydrogen bonded to a chloride anion. Thus, l^{CG} would represent the average distance between ionic and molecular nanodomains.

To verify that choline ions are indeed decoupled from the coherent dynamics of the glycerol network in glyceline, we have

DOI: 10.1021/acs.jpcb.7b11224
J. Phys. Chem. B 2018, 122, 1261–1267

computed the "combined" (CG) correlation function, shown in Figure 4, as explained in the Methods section. Such correlation

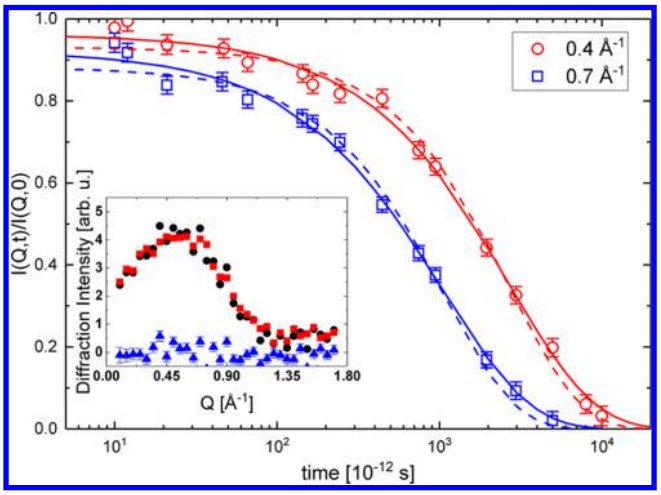

Figure 4. NSE data (318 K) computed as explained in the Methods section that describes choline–glycerol dynamic correlations. Dashed lines: fits with simple exponential decay. Solid lines: fits with stretched-exponential decay. The choice of the Q values of 0.4 and 0.7 Å^{-1} is explained in the inset that shows coherent (red squares), incoherent (blue triangles), and total (black circles) diffraction scattering signals for this correlation function.

function represents the dynamics of the choline-rich domain with respect to the glycerol-rich medium. Notice that such information could not be directly obtained from the hd or dh samples because of the non-negligible incoherent scattering contributions.

The CG NSE data could be reasonably well fitted even with a simple exponential decay, $I(t) = A \exp[-(t/\tau)]$, and the best fit with a stretched-exponential decay, $I(Q, t)/I(Q, 0) = A \exp[-(t/\tau)^{\beta}]$, yielded $A = 0.96 \pm 0.01$, $\tau = 2.68 \times 10^{-9} \pm 1.1 \times 10^{-10}$ s, $\beta = 0.83 \pm 0.04$ at $Q = 0.4$ Å^{-1} and $A = 0.92 \pm 0.01$, $\tau = 1.04 \times 10^{-9} \pm 4 \times 10^{-11}$ s, $\beta = 0.81 \pm 0.04$ at $Q = 0.7$ Å^{-1}. Note that fits of the NSE data for the dd sample at $Q = 1.4$ Å^{-1} shown in Figure 2 (which represent glycerol–glycerol correlations in glyceline, as evident from the polarized diffraction data) require significantly smaller stretching parameters, $\beta \approx 0.5$–0.6. These values are smaller than those for pure glycerol ($\beta \approx 0.7$),[64] which can be ascribed to the additional disorder in the present mixture, leading to a broader distribution of relaxation times.[67,68] The CG NSE data, on the contrary, are more indicative of uncorrelated dynamic fluctuations of the ionic and molecular nanodomains in glyceline.

CONCLUSIONS

To summarize, in spite of the large difference in viscosity between the DES glyceline and one of its parent compounds, glycerol, we have found that the structural network of glyceline is completely defined by its glycerol constituent. The dielectric relaxation times mirror the different viscosities of glyceline and glycerol. At the same time, the network dynamics in glyceline is defined by the glycerol–glycerol dynamic correlations. On the contrary, the choline–glycerol dynamic correlation function in glyceline shows largely uncorrelated fluctuations. These findings indicate that glyceline is actually a highly correlated hydrogen-bonding network of glycerol molecules, where the choline ions occupy the interstitial voids, showing little structural or dynamic correlations with the glycerol network. We conclude that in applications where the localized dynamics is essential, the local transport and dynamic properties of glyceline, counterintuitively, must be dominated by the relatively loosely bound choline ions, despite their larger size compared to that of glycerol molecules. The latter are connected in a hydrogen-bonding network that dominates the structure and collective dynamics of glyceline.

ASSOCIATED CONTENT

Supporting Information

The Supporting Information is available free of charge on the ACS Publications website at DOI: 10.1021/acs.jpcb.7b11224.

Experimental details, discussion of dielectric spectra, description of neutron spin-echo and intermediate scattering function, scheme and details for the synthesis of choline-d_{14} chloride, supplemental dielectric spectra figures (PDF)

AUTHOR INFORMATION

Corresponding Authors

*E-mail: antonio.faraone@nist.gov (A.F.).
*E-mail: bakergar@missouri.edu (G.A.B.).
*E-mail: mamontove@ornl.gov (E.M.).

ORCID

A. Faraone: 0000-0002-3783-5816
D. V. Wagle: 0000-0002-2522-0670
G. A. Baker: 0000-0002-3052-7730
P. Lunkenheimer: 0000-0002-4525-1394
E. Mamontov: 0000-0002-5684-2675

Notes

The authors declare no competing financial interest. Throughout the paper uncertainties and error bars represent one standard deviation. The identification of any commercial product or trade name does not imply endorsement or recommendation by the National Institute of Standards and Technology.

ACKNOWLEDGMENTS

This work utilized facilities supported in part by the National Science Foundation under Agreement No. DMR-1508249 and received financial support from a Research Council grant at the University of Missouri.

REFERENCES

(1) Abbott, A. P.; Capper, G.; Davies, D. L.; Rasheed, R. K.; Tambyrajah, V. Novel Solvent Properties of Choline Chloride/Urea Mixtures. *Chem. Commun.* **2003**, 70–71.

(2) Abbott, A. P.; Boothby, D.; Capper, G.; Davies, D. L.; Rasheed, R. K. Deep Eutectic Solvents Formed between Choline Chloride and Carboxylic Acids: Versatile Alternatives to Ionic Liquids. *J. Am. Chem. Soc.* **2004**, *126*, 9142–9147.

(3) Wagle, D. V.; Zhao, H.; Baker, G. A. Deep Eutectic Solvents: Sustainable Media for Nanoscale and Functional Materials. *Acc. Chem. Res.* **2014**, *47*, 2299–2308.

(4) Ge, X.; Gu, C. D.; Lu, Y.; Wang, X. L.; Tu, J. P. A Versatile Protocol for the Ionothermal Synthesis of Nanostructured Nickel Compounds as Energy Storage Materials from a Choline Chloride-Based Ionic Liquid. *J. Mater. Chem. A* **2013**, *1*, 13454–13461.

(5) Zhang, H.; Lu, Y.; Gu, C.-D.; Wang, X.-L.; Tu, J.-P. Ionothermal Synthesis and Lithium Storage Performance of Core/Shell Structured

DOI: 10.1021/acs.jpcb.7b11224
J. Phys. Chem. B 2018, 122, 1261–1267

Amorphous@Crystalline Ni-P Nanoparticles. *CrystEngComm* **2012**, *14*, 7942−7950.
(6) Wei, L.; Fan, Y.-J.; Tian, N.; Zhou, Z.-Y.; Zhao, X.-Q.; Mao, B.-W.; Sun, S.-G. Electrochemically Shape-Controlled Synthesis in Deep Eutectic Solvents—a New Route to Prepare Pt Nanocrystals Enclosed by High-Index Facets with High Catalytic Activity. *J. Phys. Chem. C* **2012**, *116*, 2040−2044.
(7) Wei, L.; Zhou, Z.-Y.; Chen, S.-P.; Xu, C.-D.; Su, D.; Schuster, M. E.; Sun, S.-G. Electrochemically Shape-Controlled Synthesis in Deep Eutectic Solvents: Triambic Icosahedral Platinum Nanocrystals with High-Index Facets and Their Enhanced Catalytic Activity. *Chem. Commun.* **2013**, *49*, 11152−11154.
(8) Morris, R. E. Ionothermal Synthesis-Ionic Liquids as Functional Solvents in the Preparation of Crystalline Materials. *Chem. Commun.* **2009**, 2990−2998.
(9) Parnham, E. R.; Morris, R. E. Ionothermal Synthesis of Zeolites, Metal−Organic Frameworks, and Inorganic−Organic Hybrids. *Acc. Chem. Res.* **2007**, *40*, 1005−1013.
(10) Cooper, E. R.; Andrews, C. D.; Wheatley, P. S.; Webb, P. B.; Wormald, P.; Morris, R. E. Ionic Liquids and Eutectic Mixtures as Solvent and Template in Synthesis of Zeolite Analogues. *Nature* **2004**, *430*, 1012−1016.
(11) Gu, C. D.; Xu, X. J.; Tu, J. P. Fabrication and Wettability of Nanoporous Silver Film on Copper from Choline Chloride-Based Deep Eutectic Solvents. *J. Phys. Chem. C* **2010**, *114*, 13614−13619.
(12) Hammons, J. A.; Muselle, T.; Ustarroz, J.; Tzedaki, M.; Raes, M.; Hubin, A.; Terryn, H. Stability, Assembly, and Particle/Solvent Interactions of Pd Nanoparticles Electrodeposited from a Deep Eutectic Solvent. *J. Phys. Chem. C* **2013**, *117*, 14381−14389.
(13) Gu, C.; Tu, J. One-Step Fabrication of Nanostructured Ni Film with Lotus Effect from Deep Eutectic Solvent. *Langmuir* **2011**, *27*, 10132−10140.
(14) Sze, L. L.; Pandey, S.; Ravula, S.; Pandey, S.; Zhao, H.; Baker, G. A.; Baker, S. N. Ternary Deep Eutectic Solvents Tasked for Carbon Dioxide Capture. *ACS Sustainable Chem. Eng.* **2014**, *2*, 2117−2123.
(15) Francisco, M.; van den Bruinhorst, A.; Zubeir, L. F.; Peters, C. J.; Kroon, M. C. A New Low Transition Temperature Mixture (Lttm) Formed by Choline Chloride + Lactic Acid: Characterization as Solvent for Co_2 Capture. *Fluid Phase Equilib.* **2013**, *340*, 77−84.
(16) Trivedi, T. J.; Lee, J. H.; Lee, H. J.; Jeong, Y. K.; Choi, J. W. Deep Eutectic Solvents as Attractive Media for Co_2 Capture. *Green Chem.* **2016**, *18*, 2834−2842.
(17) Carvalho, P. J.; Kurnia, K. A.; Coutinho, J. A. P. Dispelling Some Myths About the Co_2 Solubility in Ionic Liquids. *Phys. Chem. Chem. Phys.* **2016**, *18*, 14757−14771.
(18) Sarmad, S.; Mikkola, J.-P.; Ji, X. Carbon Dioxide Capture with Ionic Liquids and Deep Eutectic Solvents: A New Generation of Sorbents. *ChemSusChem* **2017**, *10*, 324−352.
(19) López-Salas, N.; Jardim, E. O.; Silvestre-Albero, A.; Gutiérrez, M. C.; Ferrer, M. L.; Rodríguez-Reinoso, F.; Silvestre-Albero, J.; del Monte, F. Use of Eutectic Mixtures for Preparation of Monolithic Carbons with Co_2-Adsorption and Gas-Separation Capabilities. *Langmuir* **2014**, *30*, 12220−12228.
(20) Chen, S.; Zhang, J.; Wu, T.; Feng, P.; Bu, X. Multiroute Synthesis of Porous Anionic Frameworks and Size-Tunable Extra-framework Organic Cation-Controlled Gas Sorption Properties. *J. Am. Chem. Soc.* **2009**, *131*, 16027−16029.
(21) Zhu, W.; Wang, C.; Li, H.; Wu, P.; Xun, S.; Jiang, W.; Chen, Z.; Zhao, Z.; Li, H. One-Pot Extraction Combined with Metal-Free Photochemical Aerobic Oxidative Desulfurization in Deep Eutectic Solvent. *Green Chem.* **2015**, *17*, 2464−2472.
(22) Zhao, H.; Baker, G. A.; Wagle, D. V.; Ravula, S.; Zhang, Q. Tuning Task-Specific Ionic Liquids for the Extractive Desulfurization of Liquid Fuel. *ACS Sustainable Chem. Eng.* **2016**, *4*, 4771−4780.
(23) Liu, W.; Jiang, W.; Zhu, W.; Zhu, W.; Li, H.; Guo, T.; Zhu, W.; Li, H. Oxidative Desulfurization of Fuels Promoted by Choline Chloride-Based Deep Eutectic Solvents. *J. Mol. Catal. A: Chem.* **2016**, *424*, 261−268.
(24) Pal, M.; Rai, R.; Yadav, A.; Khanna, R.; Baker, G. A.; Pandey, S. Self-Aggregation of Sodium Dodecyl Sulfate within (Choline Chloride + Urea) Deep Eutectic Solvent. *Langmuir* **2014**, *30*, 13191−13198.
(25) Sanchez-Fernandez, A.; Edler, K. J.; Arnold, T.; Heenan, R. K.; Porcar, L.; Terrill, N. J.; Terry, A. E.; Jackson, A. J. Micelle Structure in a Deep Eutectic Solvent: A Small-Angle Scattering Study. *Phys. Chem. Chem. Phys.* **2016**, *18*, 14063−14073.
(26) Tan, X.; Zhang, J.; Luo, T.; Sang, X.; Liu, C.; Zhang, B.; Peng, L.; Li, W.; Han, B. Micellization of Long-Chain Ionic Liquids in Deep Eutectic Solvents. *Soft Matter* **2016**, *12*, 5297−5303.
(27) Arnold, T.; Jackson, A. J.; Sanchez-Fernandez, A.; Magnone, D.; Terry, A. E.; Edler, K. J. Surfactant Behavior of Sodium Dodecylsulfate in Deep Eutectic Solvent Choline Chloride/Urea. *Langmuir* **2015**, *31*, 12894−12902.
(28) Gutiérrez, M. C.; Carriazo, D.; Ania, C. O.; Parra, J. B.; Ferrer, M. L.; del Monte, F. Deep Eutectic Solvents as Both Precursors and Structure Directing Agents in the Synthesis of Nitrogen Doped Hierarchical Carbons Highly Suitable for Co_2 Capture. *Energy Environ. Sci.* **2011**, *4*, 3535−3544.
(29) Gutiérrez, M. C.; Carriazo, D.; Tamayo, A.; Jiménez, R.; Picó, F.; Rojo, J. M.; Ferrer, M. L.; del Monte, F. Deep-Eutectic-Solvent-Assisted Synthesis of Hierarchical Carbon Electrodes Exhibiting Capacitance Retention at High Current Densities. *Chem. - Eur. J.* **2011**, *17*, 10533−10537.
(30) Ruβ, C.; Burkhard, K. Low Melting Mixtures in Organic Synthesis - an Alternative to Ionic Liquids? *Green Chem.* **2012**, *14*, 2969−2982.
(31) Passos, H.; Tavares, D. J. P.; Ferreira, A. M.; Freire, M. G.; Coutinho, J. A. P. Are Aqueous Biphasic Systems Composed of Deep Eutectic Solvents Ternary or Quaternary Systems? *ACS Sustainable Chem. Eng.* **2016**, *4*, 2881−2886.
(32) Zhao, H.; Baker, G. A. Ionic Liquids and Deep Eutectic Solvents for Biodiesel Synthesis: A Review. *J. Chem. Technol. Biotechnol.* **2013**, *88*, 3−12.
(33) Francisco, M.; van den Bruinhorst, A.; Kroon, M. C. New Natural and Renewable Low Transition Temperature Mixtures (Lttms): Screening as Solvents for Lignocellulosic Biomass Processing. *Green Chem.* **2012**, *14*, 2153−2157.
(34) Xia, S.; Baker, G. A.; Li, H.; Ravula, S.; Zhao, H. Aqueous Ionic Liquids and Deep Eutectic Solvents for Cellulosic Biomass Pretreatment and Saccharification. *RSC Adv.* **2014**, *4*, 10586−10596.
(35) Sharma, M.; Mukesh, C.; Mondal, D.; Prasad, K. Dissolution of [Small Alpha]-Chitin in Deep Eutectic Solvents. *RSC Adv.* **2013**, *3*, 18149−18155.
(36) Mondal, D.; Sharma, M.; Mukesh, C.; Gupta, V.; Prasad, K. Improved Solubility of DNA in Recyclable and Reusable Bio-Based Deep Eutectic Solvents with Long-Term Structural and Chemical Stability. *Chem. Commun.* **2013**, *49*, 9606−9608.
(37) Mamajanov, I.; Engelhart, A. E.; Bean, H. D.; Hud, N. V. DNA and RNA in Anhydrous Media: Duplex, Triplex, and G-Quadruplex Secondary Structures in a Deep Eutectic Solvent. *Angew. Chem., Int. Ed.* **2010**, *49*, 6310−6314.
(38) Wagle, D. V.; Deakyne, C. A.; Baker, G. A. Quantum Chemical Insight into the Interactions and Thermodynamics Present in Choline Chloride Based Deep Eutectic Solvents. *J. Phys. Chem. B* **2016**, *120*, 6739−6746.
(39) Zahn, S.; Kirchner, B.; Mollenhauer, D. Charge Spreading in Deep Eutectic Solvents. *ChemPhysChem* **2016**, *17*, 3354−3358.
(40) Wagle, D. V.; Adhikari, L.; Baker, G. A. Computational Perspectives on Structure, Dynamics, Gas Sorption, and Bio-Interactions in Deep Eutectic Solvents. *Fluid Phase Equilib.* **2017**, *448*, 50−58.
(41) Stefanovic, R.; Ludwig, M.; Webber, G. B.; Atkin, R.; Page, A. J. Nanostructure, Hydrogen Bonding and Rheology in Choline Chloride Deep Eutectic Solvents as a Function of the Hydrogen Bond Donor. *Phys. Chem. Chem. Phys.* **2017**, 3297−3306.
(42) García, G.; Atilhan, M.; Aparicio, S. An Approach for the Rationalization of Melting Temperature for Deep Eutectic Solvents from Dft. *Chem. Phys. Lett.* **2015**, *634*, 151−155.

DOI: 10.1021/acs.jpcb.7b11224
J. Phys. Chem. B 2018, 122, 1261−1267

(43) Hammond, O. S.; Bowron, D. T.; Jackson, A. J.; Arnold, T.; Sanchez-Fernandez, A.; Tsapatsaris, N.; Garcia Sakai, V.; Edler, K. J. Resilience of Malic Acid Natural Deep Eutectic Solvent Nanostructure to Solidification and Hydration. *J. Phys. Chem. B* **2017**, *121*, 7473−7483.
(44) Hammond, O. S.; Bowron, D. T.; Edler, K. J. The Effect of Water Upon Deep Eutectic Solvent Nanostructure: An Unusual Transition from Ionic Mixture to Aqueous Solution. *Angew. Chem., Int. Ed.* **2017**, *56*, 9782−9785.
(45) Kaur, S.; Gupta, A.; Kashyap, H. K. Nanoscale Spatial Heterogeneity in Deep Eutectic Solvents. *J. Phys. Chem. B* **2016**, *120*, 6712−6720.
(46) Araujo, C. F.; Coutinho, J. A. P.; Nolasco, M. M.; Parker, S. F.; Ribeiro-Claro, P. J. A.; Rudic, S.; Soares, B. I. G.; Vaz, P. D. Inelastic Neutron Scattering Study of Reline: Shedding Light on the Hydrogen Bonding Network of Deep Eutectic Solvents. *Phys. Chem. Chem. Phys.* **2017**, *19*, 17998−18009.
(47) Hammond, O. S.; Bowron, D. T.; Edler, K. J. Liquid Structure of the Choline Chloride-Urea Deep Eutectic Solvent (Reline) from Neutron Diffraction and Atomistic Modelling. *Green Chem.* **2016**, *18*, 2736−2744.
(48) Wagle, D. V.; Baker, G. A.; Mamontov, E. Differential Microscopic Mobility of Components within a Deep Eutectic Solvent. *J. Phys. Chem. Lett.* **2015**, *6*, 2924−2928.
(49) Sapir, L.; Stanley, C. B.; Harries, D. Properties of Polyvinylpyrrolidone in a Deep Eutectic Solvent. *J. Phys. Chem. A* **2016**, *120*, 3253−3259.
(50) Sanchez-Fernandez, A.; Edler, K. J.; Arnold, T.; Alba Venero, D.; Jackson, A. J. Protein Conformation in Pure and Hydrated Deep Eutectic Solvents. *Phys. Chem. Chem. Phys.* **2017**, *19*, 8667−8670.
(51) Chen, Z.; McDonald, S.; FitzGerald, P.; Warr, G. G.; Atkin, R. Small Angle Neutron Scattering Study of the Conformation of Poly(Ethylene Oxide) Dissolved in Deep Eutectic Solvents. *J. Colloid Interface Sci.* **2017**, *506*, 486−492.
(52) Sanchez-Fernandez, A.; Arnold, T.; Jackson, A. J.; Fussell, S. L.; Heenan, R. K.; Campbell, R. A.; Edler, K. J. Micellization of Alkyltrimethylammonium Bromide Surfactants in Choline Chloride:-Glycerol Deep Eutectic Solvent. *Phys. Chem. Chem. Phys.* **2016**, *18*, 33240−33249.
(53) Abbott, A. P.; Harris, R. C.; Ryder, K. S.; D'Agostino, C.; Gladden, L. F.; Mantle, M. D. Glycerol Eutectics as Sustainable Solvent Systems. *Green Chem.* **2011**, *13*, 82−90.
(54) D'Agostino, C.; Harris, R. C.; Abbott, A. P.; Gladden, L. F.; Mantle, M. D. Molecular Motion and Ion Diffusion in Choline Chloride Based Deep Eutectic Solvents Studied by 1 h Pulsed Field Gradient Nmr Spectroscopy. *Phys. Chem. Chem. Phys.* **2011**, *13*, 21383−21391.
(55) D'Agostino, C.; Gladden, L. F.; Mantle, M. D.; Abbott, A. P.; Ahmed, E. I.; Al-Murshedi, A. Y. M.; Harris, R. C. Molecular and Ionic Diffusion in Aqueous - Deep Eutectic Solvent Mixtures: Probing Inter-Molecular Interactions Using Pfg Nmr. *Phys. Chem. Chem. Phys.* **2015**, *17*, 15297−15304.
(56) Böhmer, R.; Maglione, M.; Lunkenheimer, P.; Loidl, A. Radio-Frequency Dielectric Measurements at Temperatures from 10 to 450 K. *J. Appl. Phys.* **1989**, *65*, 901−904.
(57) Schneider, U.; Lunkenheimer, P.; Pimenov, A.; Brand, R.; Loidl, A. Wide Range Dielectric Spectroscopy on Glass-Forming Materials: An Experimental Overview. *Ferroelectrics* **2001**, *249*, 89−98.
(58) Faraone, A.; Hong, K.; Kneller, L. R.; Ohl, M.; Copley, J. R. D. Coherent Dynamics of Meta-Toluidine Investigated by Quasielastic Neutron Scattering. *J. Chem. Phys.* **2012**, *136*, No. 104502.
(59) Bertrand, C. E.; Self, J. L.; Copley, J. R. D.; Faraone, A. Nanoscopic Length Scale Dependence of Hydrogen Bonded Molecular Associates' Dynamics in Methanol. *J. Chem. Phys.* **2017**, *146*, No. 194501.
(60) Lunkenheimer, P.; Kastner, S.; Köhler, M.; Loidl, A. Temperature Development of Glassy alpha-Relaxation Dynamics Determined by Broadband Dielectric Spectroscopy. *Phys. Rev. E* **2010**, *81*, No. 051504.
(61) Angell, C. A. Formation of Glasses from Liquids and Biopolymers. *Science* **1995**, *267*, 1924−1935.
(62) AlOmar, M. K.; Hayyan, M.; Alsaadi, M. A.; Akib, S.; Hayyan, A.; Hashim, M. A. Glycerol-Based Deep Eutectic Solvents: Physical Properties. *J. Mol. Liq.* **2016**, *215*, 98−103.
(63) Tomlinson, D. J. Temperature Dependent Self-Diffusion Coefficient Measurements of Glycerol by the Pulsed N.M.R. Technique. *Mol. Phys.* **1973**, *25*, 735−738.
(64) Wuttke, J.; Petry, W.; Pouget, S. Structural Relaxation in Viscous Glycerol: Coherent Neutron Scattering. *J. Chem. Phys.* **1996**, *105*, 5177−5182.
(65) Mamontov, E.; Ohl, M. Slow Dynamics of Water Molecules in an Aqueous Solution of Lithium Chloride Probed by Neutron Spin-Echo. *Phys. Chem. Chem. Phys.* **2013**, *15*, 10732−10739.
(66) Lunkenheimer, P.; Schneider, U.; Brand, R.; Loidl, A. Glassy Dynamics. *Contemp. Phys.* **2000**, *41*, 15−36.
(67) Sillescu, H. Heterogeneity at the Glass Transition: A Review. *J. Non-Cryst. Solids* **1999**, *243*, 81−108.
(68) Ediger, M. D. Spatially Heterogeneous Dynamics in Supercooled Liquids. *Annu. Rev. Phys. Chem.* **2000**, *51*, 99−128.

DOI: 10.1021/acs.jpcb.7b11224
J. Phys. Chem. B 2018, 122, 1261−1267